*Inorg. Chem.* **2006**, *45*, 6404–6410


# Low-Temperature Synthesis of α-$MnO_2$ Hollow Urchins and Their Application in Rechargeable $Li^+$ Batteries

**Benxia Li,[†] Guoxin Rong,[†] Yi Xie,*[,†] Lunfeng Huang,[‡] and Chuanqi Feng[‡]**

*Nanomaterial & Nanochemistry, Hefei National Laboratory for Physical Sciences at Microscale, University of Science and Technology of China, Hefei, Anhui 230026, People's Republic of China, and Department of Chemistry and Materials Science, Hubei University, Wuhan, Hubei 430062, People's Republic of China*

Received April 13, 2006

Novel α-$MnO_2$ hollow urchins were synthesized on a large scale by a facile and efficient low-temperature (60 °C) mild reduction route, without templates or surfactants in the system. The formation mechanism for the hollow urchins was proved to be the Ostwald ripening process by tracking the crystallization and morphology of the product at different reaction stages. The as-prepared hollow-urchin sample has a high Brunauer–Emmett–Teller surface area of 132 $m^2/g$ and a mesoporous structure, which were expected to help improve the electrochemical property in $Li^+$ batteries. When the α-$MnO_2$ hollow urchins were used as the cathode material in Li batteries, they performed better than the other α-$MnO_2$ samples (solid urchins and dispersed nanorods), indicating that the electrochemical performance of the electrode material is sensitive to its morphology. This synthetic procedure is straightforward and inexpensive and thus facilitates mass production of α-$MnO_2$ hollow urchins.

## 1. Introduction

Hollow structures with nano- or microscale sizes have attracted much attention as a special class of materials because of their unique properties, including high specific surface area, low density, and good permeation, and potential applications in catalysts, protection of light-sensitive components, artificial cells, and controlled release of drugs.[1] Usually, hollow spheres are fabricated using various template precursors, such as spherical silica,[2] polystyrene spheres,[3] micelles,[4] liquid droplets,[5] macromolecular micelles.[6] These preparations often require removal of the templates after synthesis utilizing separation methods such as acid or base etching and calcinations, which may damage the desired configurations of the hollow spheres. Most of the hollow spheres prepared previously were mainly congregated by nanoparticles and exhibited polycrystalline characteristics. However, one-dimensional (1D) nanostructures have been demonstrated to possess superior electrical, optical, and mechanical properties, suggesting their potential applications as building blocks in microscaled devices.[7] For novel technologies based on nanoscale devices, we need not only to prepare 1D nanomaterials but also to try to organize them into well-aligned patterns of configurations, which is of great interest in areas of chemistry and materials science.[8] The hollow structures with nano- or microscale sizes assembled by well-crystalline 1D nanoscale building blocks are pursued and expected to provide the materials' novel and unexpected properties.[9] α-$MnO_2$, constructed from double chains of octahedral [$MnO_6$] forming 2 × 2 tunnels, is widely used as catalysts, ion−molecular sieves, and electrode materials in

* To whom correspondence should be addressed. E-mail: yxie@ustc.edu.cn. Tel and Fax: 86-551-3603987.
[†] University of Science and Technology of China.
[‡] Hubei University.

(1) (a) Huang, H.; Remsen, E. E. *J. Am. Chem. Soc.* **1999**, *121*, 3805. (b) Zhong, Z.; Yin, Y.; Gates, B.; Xia, Y. *Adv. Mater.* **2000**, *12*, 206. (c) Bourlinos, A. B.; Karakassides, M. A.; Petridis, D. *Chem. Commun.* **2001**, 1518. (d) Zhang, D.; Qi, L.; Ma, J.; Cheng, H. *Adv. Mater.* **2002**, *14*, 1499.
(2) Chang, S. Y.; Liu, L. S.; Asher, A. *J. Am. Chem. Soc.* **1994**, *116*, 6745.
(3) Caruso, R. A.; Susha, A.; Caruso, F. *Chem. Mater.* **2001**, *13*, 400.
(4) Schmidt, H. T.; Ostafin, A. E. *Adv. Mater.* **2002**, *14*, 532.
(5) Walsh, D.; Mann, S. *Nature* **1995**, *377*, 320.
(6) Liu, T.; Xie, Y.; Chu, B. *Langmuir* **2000**, *16*, 9015.
(7) (a) Xia, Y. N.; Yang, P. D.; Sun, Y. G.; Wu, Y. Y.; Mayers, B.; Gates, B. *Adv. Mater.* **2003**, *15*, 353. (b) Wong, E. W.; Sheehan, P. E.; Lieber, C. M. *Science* **1997**, *277*, 1971. (c) Hu, J. T.; Odom, T. W.; Lieber, C. M. *Acc. Chem. Res.* **1999**, *32*, 435. (d) Dekker, C. *Phys. Today* **1999**, *52*, 22.
(8) (a) Shi, H. T.; Qi, L. M.; Ma, J. M.; Cheng, H. M. *J. Am. Chem. Soc.* **2003**, *125*, 3450. (b) Cao, X. B.; Xie, Y.; Li, L. Y. *Adv. Mater.* **2003**, *15*, 1914.



10.1021/ic0606274 CCC: $33.50 
Published on Web 07/07/2006

$Li/MnO_2$ batteries.[10] α-$MnO_2$'s well-controlled dimensionality and crystallinity have also been regarded as critical factors that may bring some novel properties. However, over the past several years, most of the as-synthesized α-$MnO_2$ nanostructures are merely nanorods and nanowires.[11,12] Recently, our group has prepared a core−shell structure of α-$MnO_2$ with nanorods assembled into shell through a solution-based catalytic route.[13] Novel α-$MnO_2$ hollow structures assembled by well-crystalline nanorods may act as catalytic microreactors, give an ideal host material for the intercalation and deintercalation of Li ions, and provide the possibility of efficient transport of electrons in the Li batteries. Thus, the synthesis of α-$MnO_2$ hollow spheres assembled by well-crystalline nanorods is desirable and significative.

For the purpose of future applications, it is doubtless that the primary objective should lie in developing various convenient synthetic strategies to obtain new nanostructures with novel shapes. Because of its easily controllable reaction condition and the relatively cheap reactant sources, the low-temperature synthesis in an aqueous solution without any organic additive is highly desirable and represents an environmentally kind and user-friendly approach, which may be considered to be a relatively green chemical alternative of practical significance.[14] In our study, it was found that a $KMnO_4$ solution and metal Cu can mildly react at room temperature according to following two half-reactions.

$$Cu^{2+} + 2e^- = Cu\ (\varphi^\circ = +0.337\ V) \quad (1)$$

$$MnO_4^- + 4H^+ + 3e^- = MnO_2 + 2H_2O\ (\varphi^\circ = +1.695\ V) \quad (2)$$

We provide a simple and efficient low-temperature (60 °C) mild reduction route to fabricate hollow urchins of α-$MnO_2$ on a large scale, without templates or surfactants in the reaction system. Hollow interiors can be created in 100% morphological yield via Ostwald ripening after a reaction time of about 8 h, and the ripening process was confirmed by tracking the crystallization and morphology of the product at different reaction stages. Moreover, the electrochemical $Li^+$ intercalation capacities of the as-obtained α-$MnO_2$ materials were investigated by using the as-prepared samples as the cathode materials in Li batteries under a constant current density of 270 mA/g. It is found that α-$MnO_2$ hollow urchins exhibited a better electrochemical property and discharged with a high capacity of 746.0 mAh/g in the first charge−discharge process, which can be explained by the high surface area and mesoporous nature of α-$MnO_2$ hollow urchins, suggesting that the electrochemical performance is sensitive to the morphologies of the materials.

## 2. Experimental Section

**Synthesis.** All chemical reagents in this work were analytical grade and were used as received. In a typical procedure, 2.0 mmol of potassium permanganate ($KMnO_4$) was dissolved in 40 mL of distilled water to form a homogeneous solution in a jar of 100 mL, and 2 mL of sulfuric acid (98 wt %) was slowly dropped into the solution and stirred for 5 min. Then, the Cu foil (2 × 8 cm) was inserted in the solution after being rinsed by dilute sulfuric acid and distilled water. The jar containing the reaction solution was kept static at 60 °C for 8 h. After the reactions, the residual Cu foil was removed from the jar and the precipitates were washed with dilute sulfuric acid and distilled water several times. The final products were dried at 50 °C for 6 h under vacuum.

**Characterization.** The products were characterized with a range of analytical techniques. In detail, X-ray diffraction (XRD) analyses were performed using a Japan Rigaku D/max-χA X-ray diffractometer equipped with graphite-monochromatized high-intensity Cu Kα radiation ($\lambda = 1.541\ 78$ Å). X-ray photoelectron spectroscopy (XPS) measurements were performed on a VGESCALAB MKII X-ray photoelectron spectrometer with an exciting source of Mg Kα = 1253.6 eV. Field-emission scanning electron microscopy (FESEM) images were taken on a JEOL JSM-6700F SEM. Transmission electron microscopy (TEM) images were taken on a Hitachi model H-800 instrument with a W filament, using an accelerating voltage of 200 kV. The high-resolution TEM (HRTEM) images and the corresponding selected-area electron diffraction (SAED) patterns were taken on a JEOL 2010 HRTEM performed at 200 kV. The nitrogen adsorption and desorption isotherms at 77 K were measured using a Micromeritics ASAP 2000 system after the sample was degassed in a vacuum at 130 °C overnight.

**Electrochemical Measurements.** The electrochemical measurements were carried out using the as-prepared model test cells. Test electrodes were prepared by mixing as-prepared $MnO_2$ samples (64−70 wt %), acetylene black (20−24 wt %), and poly(tetrafluoroethylene) (10−12 wt %). An amount of 10−20 mg of the mixture was pressed onto a Ni grid. The electrodes were dried at 120−130 °C in a vacuum furnace for 24 h before use, and Li foil was used as an anode. The model test cells were fitted together in a glovebox under an argon atmosphere. The electrolyte was a solution of 1 M $LiClO_4$ in ethylene carbonate (EC)−propylene carbonate (PC) (1:1 mol %). For long-term cycling experiments, the cells were charged and discharged between 0.01 and 2.0 V (vs $Li/Li^+$), using a constant current density of 270 mA/g. The electrochemical measurement was carried out using the Newware battery testing system (Newware BTS-5V/5 mA).

## 3. Results and Discussion

The phase and purity of the sample were identified by XRD measurement, and the XRD pattern of the final product is shown in Figure 1a. All of the diffraction peaks in the XRD pattern can be readily indexed to the pure tetragonal phase of α-$MnO_2$ (JCPDS 44-0141), indicating high purity and crystallinity of the final sample. Further evidence for the composition of the sample is obtained by XPS measurement, which is an excellent technique for understanding the

(9) (a) Goldberger, J.; He, R.; Zhang, Y.; Lee, S.; Yan, H.; Cho, H. J.; Yang, P. *Nature* **2003**, *422*, 599. (b) Cao, A. M.; Hu, J. S.; Liang, H. P.; Wan, L. J. *Angew. Chem., Int. Ed.* **2005**, *44*, 4391.
(10) (a) Yamamoto, S.; Matsuoka, O.; Fukada, I.; Ashida, Y.; Honda, T.; Yamamoto, N. *J. Catal.* **1996**, *159*, 401. (b) Horn, Y. S.; Hackney, S. A.; Johnsom, C. S.; Thackeray, M. M. *J. Electrochem. Soc.* **1998**, *145*, 582. (c) Tanaka, Y.; Tsuji, M.; Tamaura, Y. *Phys. Chem. Chem. Phys.* **2000**, *2*, 1473.
(11) (a) Wang, X.; Li, Y. D. *J. Am. Chem. Soc.* **2002**, *124*, 2880. (b) Wang, X.; Li, Y. *Chem. Commun.* **2002**, *124*, 764.
(12) Xiong, Y. J.; Xie, Y.; Li, Z. Q.; Wu, C. Z. *Chem.—Eur. J.* **2003**, *9*, 1645.
(13) Li, Z. Q.; Ding, Y.; Xiong, Y. J.; Yang, Q.; Xie, Y. *Chem. Commun.* **2005**, 918.
(14) (a) Peng, X. *Chem.—Eur. J.* **2002**, *8*, 335. (b) Zhao, N.; Qi, L. *Adv. Mater.* **2006**, *18*, 359.

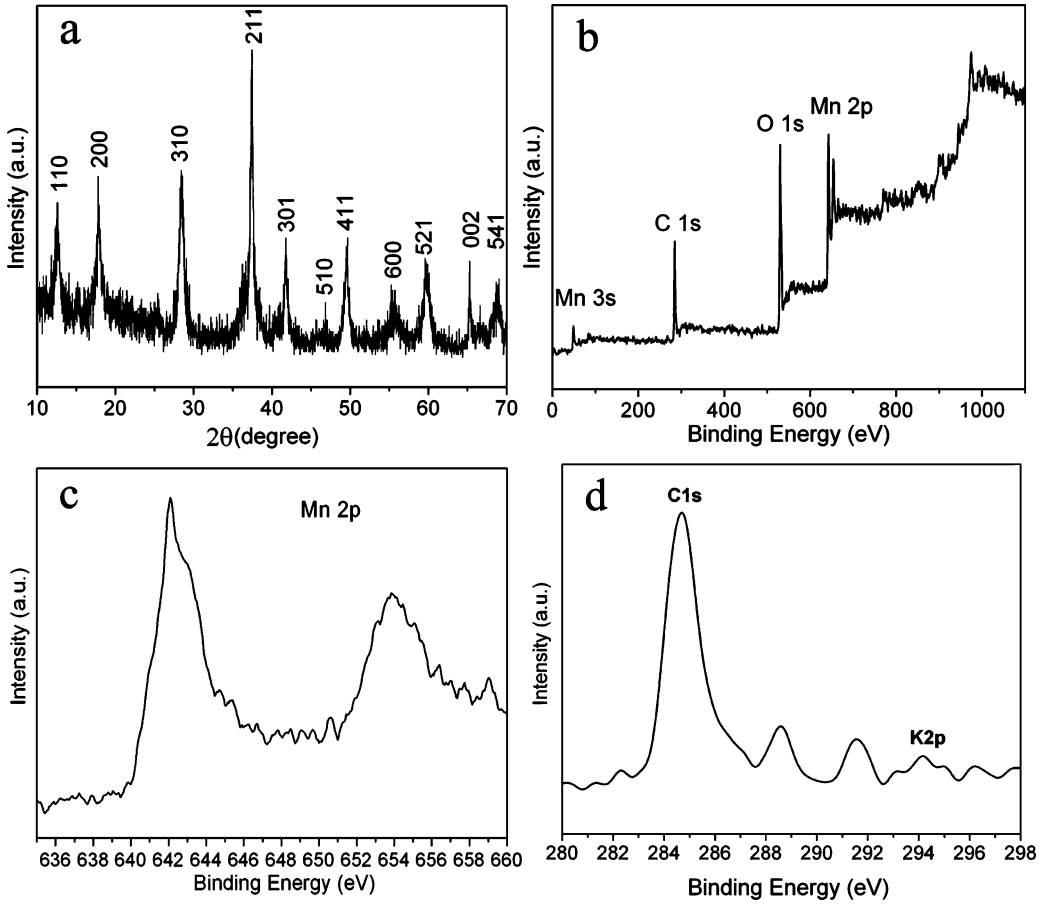


**Figure 1.** (a) XRD pattern, (b) XPS survey spectrum, (c) XPS higher-resolution spectrum of the Mn 2p region, and (d) XPS higher-resolution spectrum of the C (K) region of the product obtained at 60 °C for 8 h.

oxidation state of the transition-metal ion and the relative composition of the synthesized material. The binding energies in the XPS analysis were corrected for specimen charging by referencing the C 1s to 284.60 eV. The survey spectrum (Figure 1b) indicates the presence of Mn and O as well as C from the reference and the absence of impurity such as Cu and $Cu^{2+}$. The higher-resolution spectrum of Mn 2p in Figure 1c clearly shows that Mn $2p_{3/2}$ and $2p_{1/2}$ are found to be 642 and 654 eV, respectively. The values agree well with those reported for $MnO_2$,[15] indicating that the oxidation state is 4+. In addition, a peak at about 294 eV attributed to K 2p of $K^+$ is observed in the higher-resolution spectrum of the C region in Figure 1d, but the peak is extremely weak and the content of element K in the product is calculated to be 0.84 atom %, which is so low that it cannot be observed in the XPS survey spectrum and XRD pattern. Thus, the crystal structure of the sample has more sites to accommodate $Li^+$, facilitating the potential application for electrode material in Li batteries.

The morphology of the α-$MnO_2$ product obtained through the mild reduction route was illuminated by FESEM images, as shown in Figure 2. Figure 2a shows a panoramic FESEM image of the product, which is composed of uniform microspheres and is present in high quantity. A magnified FESEM image of the sample in Figure 2b indicates that these α-$MnO_2$ microspheres look like some natural urchins, with diameters of 1−3 $\mu$m and numerous nanorods compactly growing around their surfaces. Moreover, these urchins exhibit interesting hollow structures, and the cavities can be clearly seen from the FESEM observation. Thus, the obtained α-$MnO_2$ structures are called hollow urchins. Figure 2c displays a representative open hollow urchin with a diameter of about 2.0 $\mu$m, the shell of which is formed by the densely aligned nanorods with uniform diameters of about 30 nm and lengths of 200−300 nm. The hollow interior occupies 70−90% by volume in an urchin. The product was further investigated by HRTEM, in which the sample was treated by ultrasonic dispersion in ethanol for 10 min and then dropped on a Cu mesh. The TEM and HRTEM images (Figure 2d,e) of a single nanorod from a hollow urchin indicate that the nanorod is structurally uniform and crystalline; the lattice spacing of 0.69 nm is consistent with that of the α-$MnO_2$ (110) plane. Meanwhile, the electron diffraction pattern (inset in Figure 2d) can be indexed to be the $[1\bar{1}0]$ zone axis of α-$MnO_2$, further confirming that the nanorods are crystalline and grow along the [001] axis.

In our approach, the Cu foil was used as a mild reducing reagent to slow the precipitation of α-$MnO_2$, which is necessary to assemble into the hollow urchins; such structures have not been obtained using other reducing reagents.[16] The

(15) Subramanian, V.; Zhu, H. W.; Vajtai, R.; Ajayan, P. M.; Wei, B. Q. *J. Phys. Chem. B* **2005**, *109*, 20207.

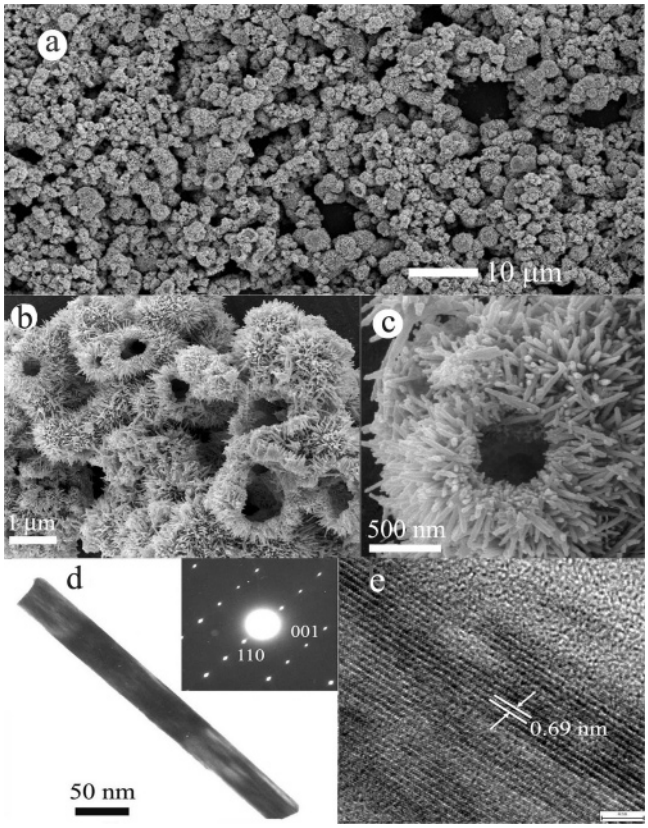


**Figure 2.** (a) Panoramic FESEM image, (b) magnified FESEM image, (c) typical open hollow urchin of the product obtained at 60 °C for 8 h, (d) TEM image of a nanorod from the hollow urchins (inset: SAED pattern taken from the nanorod), and (e) HRTEM image from the nanorod.

chemical reaction in this system for the synthesis of α-$MnO_2$ hollow urchins can be formulated as eq 3. To easily remove

$$2KMnO_4 + 3Cu + 4H_2SO_4 = 2MnO_2 + 3CuSO_4 + K_2SO_4 + 4H_2O \quad (3)$$

the residual metal Cu from the product of $MnO_2$, Cu foil, instead of Cu powder, was used here.

In this synthesis method, neither templates nor surfactants were used. For a complete view of the formation process of α-$MnO_2$ hollow urchins and their growth mechanism, detailed time-dependent evolutions of morphology and crystallinity at 60 °C were studied by TEM and XRD measurements, which are shown in Figure 3. During the experiments, it was observed that the color of the $KMnO_4$ solution disappeared after 1 h and the colloids were precipitated from the solution; as shown in Figure 3a, the sample obtained at this time contains spherical colloidal aggregations with diameters of 200−500 nm. It is noteworthy that the $MnO_2$ colloids were precipitated in the solution rather than attached on the surface of the Cu foil. When the reaction time is prolonged to 3 h, as shown in Figure 4b, many nanorods with diameters of about 20 nm and lengths of about 100 nm grew from the colloidal spheres and formed solid urchins. After 5 h of reaction (Figure 3c), the diameters and

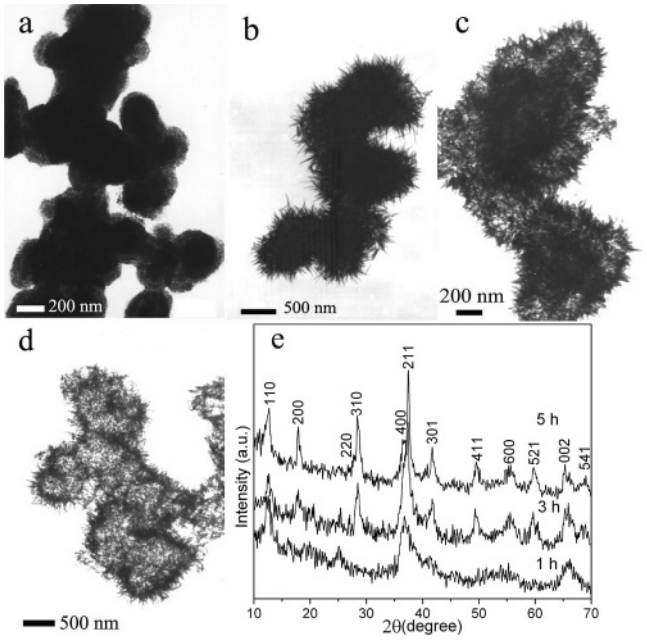


**Figure 3.** TEM images of the products obtained at 60 °C for different reaction times: (a) 1 h, (b) 3 h, (c) 5 h, (d) 8 h. (e) XRD patterns of the products from different reaction stages.

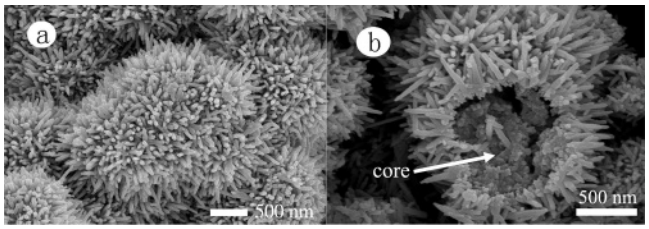


**Figure 4.** FESEM images of the samples obtained at the reaction stages of (a) 3 h and (b) 5 h, respectively.

lengths of the nanorods on the solid urchins increased to 30 and 200 nm, respectively; the cores in the spheres were shrinking to form incompletely hollow urchins. For 8 h of reaction (Figure 3d), the product consists predominantly of hollow urchins, with their cores disappearing completely. XRD patterns of the samples obtained at different stages (Figure 3e) display the gradual increase of the crystallinity of α-$MnO_2$ products. The product after 8 h of reaction exhibits good crystallinity, as revealed by its XRD and SAED patterns. In addition, FESEM images of the 3- and 5-h samples (Figure 4) further confirmed that solid urchins were formed after 3 h of reaction and the partly hollow urchins were formed after 5 h. The broken urchin in Figure 4b also illuminates that the residual cores in the partly hollow urchins are congregated by tiny particles.

On the basis of the above evolution of the time-dependent crystallinity and morphology, the formation process of the hollow urchins was illustrated in Scheme 1. In the initial stage, $MnO_2$ colloids were produced and aggregated to microspheres through the reaction between a $KMnO_4$ solution and a Cu foil. As $KMnO_4$ was consumed completely, the whole system was transferred to a thermodynamically stable environment. Then, because of the 1D growth habit of the α-$MnO_2$ crystal,[11] nanorods were epitaxially grown along

(16) (a) Tsang, C.; Kim, J.; Manthiram, A. *J. Solid State Chem.* **1998**, *137*, 28. (b) Ye, C.; Lin, Z. M.; Yan, J. X. *Solid State Commun.* **2005**, *133*, 121.

**Scheme 1.** Schematic Illustration of the Formation of α-$MnO_2$ Hollow Urchins via the Ostwald Ripening Process

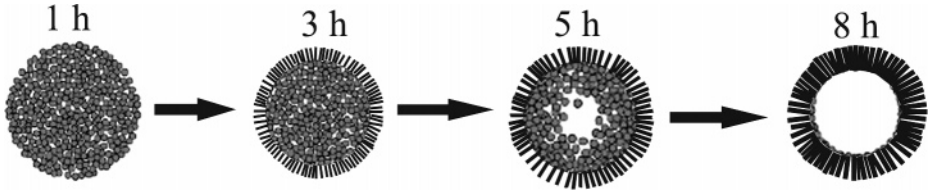


[001] from the initial colloidal microspheres and formed the solid urchins, as indicated by the sample at early stages (3 h). In addition, the crystallites located in the inner cores, compared to those in the outer surfaces, have high surface energies and thus are easily dissolved. The nanorods located on the outside would serve as starting points (or nucleation seeds) for the subsequent crystallization process of the cores. The polycrystalline cores provided a $MnO_2$ source for the durative growth of the nanorods outside during the solid evacuation, and the net result of the following events should be the nanorods growing at the expense of the cores inside the spheres. As a result of this process, the size of the polycrystalline core was reduced gradually while the hollow volume was enlarged. Finally, the hollow urchins were formed with complete depletion of the cores. A hollowing effect was observed for those with a longer reaction time (5−8 h), and the inner space of the spheres was further increased. Meanwhile, the diameters and lengths of the nanorods outside were growing wider and longer. In particular, the crystallinity of the products was increased gradually with the reaction time. All of these experimental results indicate that the underlying mechanism for the formation of hollow urchins is the well-known "Ostwald ripening process", in which the initial formation of tiny crystalline nuclei in a supersaturated medium is followed by crystal growth and the larger particles grow at the cost of the small ones because of the energy difference between them.[17] Such a similar ripening process has occurred for the creation of $TiO_2$ hollow spheres in Zeng's previous work.[18] Under the present conditions for the synthesis of α-$MnO_2$ hollow urchins, the chemical reaction between $KMnO_4$ and Cu was completed in a relatively short time of about 1 h, and the ripening process for the formation of hollow urchins took a longer time of about 7 h.

The reaction temperature seems important for the fabrication of the titled nanostructures. Most probably, a kinetic control is needed to form the hollow urchins by the Ostwald ripening process. The experiment carried out at room temperature displayed that the purple color of the $KMnO_4$ solution disappeared completely after 3 h, but the product obtained at room temperature even after 24 h (Figure 5a,b) was only composed of solid urchins with very thin nanorods on the surfaces and its XRD pattern shows poor crystalline characteristics, suggesting that the hollowing (ripening) process needs a far longer time at room temperature. However, at temperatures higher than 100 °C under hydrothermal conditions for 8 h, the ripening process proceeded at a rather higher rate, which is also not suitable for the preparation of hollow urchins. For example, the product obtained at 120 °C was well-dispersed crystalline nanorods with diameters of 50−100 nm and lengths of ∼500 nm, as depicted in Figure 5c,d. The comparative experiments indicate that the appropriate reaction temperature for the preparation of α-$MnO_2$ hollow urchins is about 60 °C.

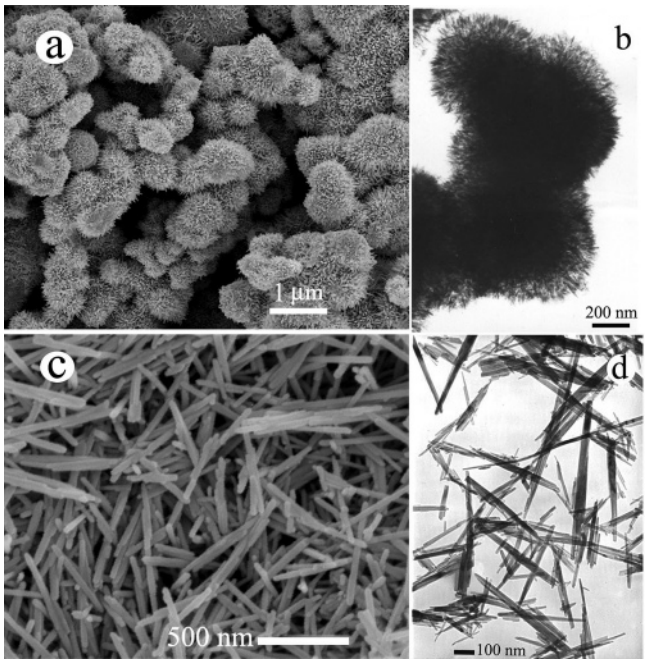


**Figure 5.** (a) FESEM image and (b) TEM image of the solid urchins obtained at room temperature for 24 h. (c) FESEM image and (d) TEM image of the dispersed nanorods obtained under 120 °C hydrothermal conditions for 8 h.

In the recent 10 years, $MnO_2$ has attracted much attention as a cathode electrode for Li batteries because of its lower cost and lower toxicity.[19] To study the potential of the α-$MnO_2$ hollow urchins as an electrode material in Li batteries and the effect of morphology on the capacity of the electrode, the charge−discharge curves of the as-prepared α-$MnO_2$ samples with different morphologies—hollow urchins (obtained at 60 °C for 8 h), solid urchins (obtained at room temperature after 24 h), and dispersed nanorods (obtained at 120 °C under hydrothermal conditions for 8 h)—were measured in the voltage range of 0.01−2.0 V vs $Li^+$/Li at a constant current density of 270 mA/g. Figure 6a shows the voltage−capacity curves of the α-$MnO_2$ samples with different morphologies as cathode materials in the first charge−discharge cycle. Notably, for the α-$MnO_2$ hollow

(17) Ostwald, W. Z. *Phys. Chem.* **1900**, *34*, 495.
(18) Yang, H. G.; Zeng, H. C. *J. Phys. Chem. B* **2004**, *108*, 3492.
(19) (a) Pistoia, G.; Wang, G. *Solid State Ionics* **1993**, *66*, 135. (b) Armstrong, A.; Bruce, P. G. *Nature* **1996**, *381*, 499. (c) Thackeray, M. M. *Prog. Batteries Battery Mater.* **1995**, *14*, 1.

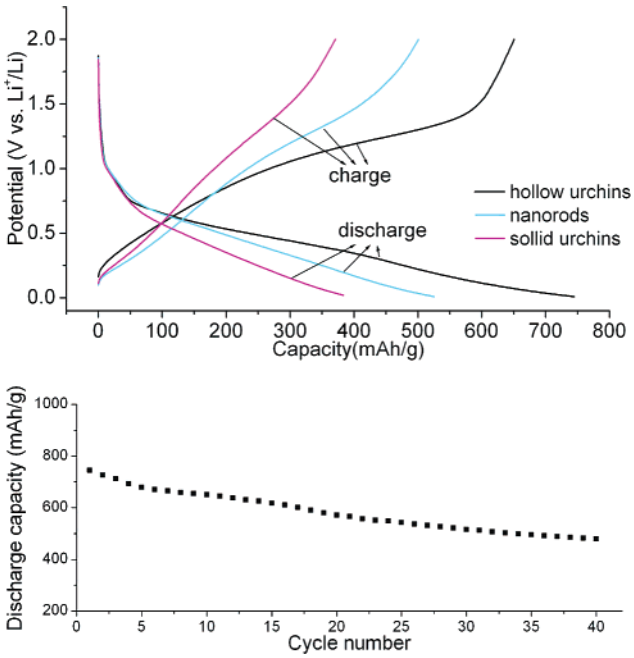


**Figure 6.** (a) Charge−discharge curves of α-$MnO_2$ hollow urchins (black lines), dispersed nanorods (cyan lines), and solid urchins (magenta lines) at a constant current density of 270 mA/g. (b) Cycle performance of the electrode from α-$MnO_2$ hollow urchins.

urchins, a high capacity of 746.0 mA·h/g was obtained in the first discharge process, while the discharge capacities of solid urchins and dispersed nanorods are 384.3 and 528.1 mA·h/g, respectively. The results suggest that the special morphology of α-$MnO_2$ hollow urchins has a remarkable effect on its electrochemical performance in Li batteries. According to the charge−discharge behaviors of transition-metal oxides, the subsequent discharge capacity considerably decayed under high current density because of the structural or textural fracture of the materials.[20] Compared with other nanoscale-sized $Li_xMnO_2$ cathodes reported previously,[21] the present α-$MnO_2$ hollow urchins, as indicated by the cycling performance in Figure 6b, exhibited a good cycle performance under such a very high current density of 270 mA/g, and the capacity of the 40th cycle remains as 481 mA·h/g, suggesting its structural stability during the charge−discharge process.

The $Li^+$'s intercalation and deintercalation process can be described by eq 4. In the present case, the redox process is

$$xLi^+ + MnO_2 + xe^- \leftrightarrow Li_xMnO_2 \qquad (4)$$

governed by the intercalation and deintercalation of $Li^+$ from the electrolyte into the porous α-$MnO_2$ matrix. It is well-known that the particle size and the surface area of the electrode dramatically affect the $Li^+$ intercalation rate and

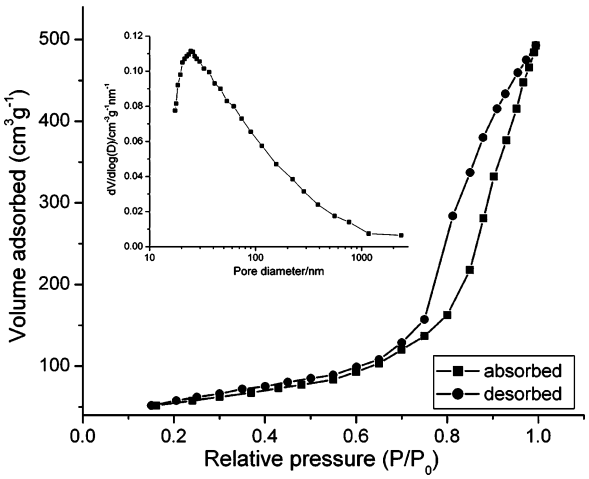


**Figure 7.** $N_2$ adsorption−desorption isotherm and BJH pore-size distribution plot (inset) of α-$MnO_2$ hollow urchins.

capacity. A high surface area can reduce the $Li^+$ intercalation rate density per unit area, which also delays the capacity loss associated with the concentration polarization to higher current density. Thus, identifying the specific surface area and pore structure of the hollow urchins is essential to understanding its higher capacity. Figure 7 shows the $N_2$ adsorption−desorption isotherm and the Barrett−Joyner−Halenda (BJH) pore-size distribution curve (inset) of α-$MnO_2$ hollow urchins. The isotherms are identified as type IV, which is characteristic of mesoporous materials.[22] The pore-size distribution, calculated from the isotherm using the BJH model, indicates that the narrow distribution of the micropores is around 25 nm in the sample. The Brunauer−Emmett−Teller (BET) specific surface area of the sample calculated from $N_2$ adsorption is 132 $m^2/g$, which is much larger than those of the solid urchins (86 $m^2/g$) and the dispersed nanorods (93 $m^2/g$). The special high BET surface area and mesoporous structure of the hollow urchins provide the possibility of efficient transport of electrons in the Li batteries, which leads to the high electrochemical capacity of hollow urchins.

## 4. Conclusions

In summary, a facile and efficient low-temperature (60 °C) solid-solution reaction route was provided to fabricate novel α-$MnO_2$ hollow urchins on a large scale, without templates or surfactants in the reaction system. The formation mechanism for the hollow urchins was proved to be the Ostwald ripening process by tracking the crystallization and morphology of the product at different reaction stages using XRD measurement and the TEM technique. Moreover, the optimal condition for the formation of the hollow urchins was confirmed by varying the reaction conditions. The reported synthetic procedure is straightforward and inexpensive, facilitating mass production of α-$MnO_2$ hollow urchins. The electrochemical study of the samples with different morphologies indicated that the discharge capacity of the

(20) (a) Poizot, P.; Laruelle, S.; Grugeon, S.; Dupont, L.; Tarascon, J. M. *Nature* **2000**, *407*, 496. (b) Wu, M. S.; Chiang, P. C.; Lee, J. T. *J. Phys. Chem. B* **2005**, *109*, 23279.

(21) (a) Kumar, G. V.; Gnanaraj, J. S.; David, B. S.; Pickup, D. M.; Eck, R. H.; Gedanken, A.; Aurbach, D. *Chem. Mater.* **2003**, *15*, 4211. (b) Ma, R.; Bando, Y.; Zhang, L.; Sasaki, T. *Adv. Mater.* **2004**, *16*, 918. (c) Watanabe, T.; Zhou, H. S.; Honma, I. *J. Electrochem. Soc.* **2005**, *152* (8), A1568. (d) Sakai, N.; Ebina, Y.; Takada, K.; Sasaki, T. *J. Electrochem. Soc.* **2005**, *152* (12), E384.

(22) Vinu, A.; Sawant, D. P.; Ariga, K.; Hartmann, M.; Halligudi, S. B. *Microporous Mesoporous Mater.* **2005**, *80*, 195.

electrode material is sensitive to the morphology. α-$MnO_2$ hollow urchins discharged with a high capacity of 746 mA·h/g in the first charge−discharge process, which may be attributed to its high surface area of 132 $m^2$/g and mesoporous structure. The present electrode material of α-$MnO_2$ hollow urchins also exhibited a good cycle performance under a high current density of 270 mA/g. These results indicate that α-$MnO_2$ hollow urchins provide a new candidate for the application for $Li^+$ batteries.

**Acknowledgment.** The financial support of this work by the National Natural Science Foundation of China is gratefully acknowledged.

IC0606274